Monthly Notices
of the
ROYAL ASTRONOMICAL SOCIETY

MNRAS **483,** 381–391 (2019)
Advance Access publication 2018 November 16

doi:10.1093/mnras/sty3081

Ion irradiation of N_2O ices and NO_2:N_2O_4 ice mixtures: first steps to understand the evolution of molecules with the N–O bond in space

Daniele Fulvio [1]★ G. A. Baratta,[2] B. Sivaraman,[3] N. J. Mason,[4] E. F. da Silveira,[1] A. L. F. de Barros [5] O. Pandoli,[6] G. Strazzulla[2] and M. E. Palumbo[2]

[1]*Departamento de Física, Pontifícia Universidade Católica do Rio de Janeiro, Rua Marquês de São Vicente 225, 22451-900 Rio de Janeiro, RJ, Brazil*
[2]*INAF-Osservatorio Astrofisico di Catania, Via Santa Sofia 78, I-95123 Catania, Italy*
[3]*Atomic Molecular and Optical Physics Division, Physical Research Laboratory, Ahmedabad 380 009, India*
[4]*Department of Physics and Astronomy, The Open University, Walton Hall, Milton Keynes MK7 6AA, UK*
[5]*Departamento de Física, Centro Federal de Educação Tecnológica Celso Suckow da Fonseca, Av. Maracanã 229, 20271-110 Rio de Janeiro, RJ, Brazil*
[6]*Departamento de Quimica, Pontifícia Universidade Católica do Rio de Janeiro, Rua Marquês de São Vicente 225, 22451-900 Rio de Janeiro, RJ, Brazil*

Accepted 2018 November 6. Received 2018 November 2; in original form 2018 September 19

ABSTRACT

Astronomical observations towards star-forming regions have revealed the presence of molecules with the N—O bond such as NO, N_2O, and HNO. These species are considered potential precursors of prebiotic molecules. Thus, understanding nitrogen and oxygen chemistry may help us to better understand the origin and evolution of prebiotic molecules in space. However, species with the N—O bond are poorly studied and laboratory works on the effects induced on them by solar wind and galactic cosmic rays are still scarce. For this, we wanted to study the effects of ion bombardment on molecules with the N—O bond. We focus here on N_2O ices and NO_2:N_2O_4 = 1:1 ice mixtures (at 16 and 50/60 K) irradiated with 200 keV protons. Infrared transmission spectroscopy (8000−500 cm^{-1}; 1.25−20 μm) was used to analyse the samples. Irradiation of N_2O ices and NO_2:N_2O_4 ice mixtures produces comparable effects independent of the irradiation temperature, NO being the main product. Moreover, we show that the maximum amount of N_2O and N_2O_4 destroyed by irradiation, at the highest dose reached in our experiments, is equal to about 98 and 70 per cent, respectively. The dose range covered in the experiments has been compared with the astrophysical time-scale of surface processing in space, showing that irradiation of N_2O and NO_2:N_2O_4 mixtures can produce, within 10^5–10^8 yr, amounts of solid NO ice detectable towards star-forming regions by the *James Webb Space Telescope*.

Key words: astrochemistry – methods: laboratory – techniques: spectroscopic – Kuiper belt: general – cosmic rays – ISM: molecules.

1 INTRODUCTION

In dense clouds of the interstellar medium (ISM), dust grains covered by ices experience a plethora of chemico-physical processes, among which are accretion and subsequent reaction of gas-phase species, reactions induced by photon and ion irradiation, thermal processing, and desorption of ices from the dust grain surface (see for instance Palumbo & Strazzulla 1993; Gerakines, Schutte & Ehrenfreund 1996; Kaiser & Roessler 1998; Charnley, Rodgers & Ehrenfreund 2001; Cottin et al. 2008; Raut et al. 2008, 2012; Öberg et al. 2011; Fulvio, Raut & Baragiola 2012; Garrod & Weaver 2013; Qi et al. 2013; Boogert, Gerakines & Whittet 2015; Fulvio et al. 2017).

Molecules containing nitrogen and oxygen with the N—O bond (hereinafter N—O species) are considered potential precursors of prebiotic molecules therefore understanding their chemical evolution in space is matter of great interest. However, to date, few N—O species have been identified in the ISM and then only in gas-phase – NO, N_2O, and HNO found in star - forming regions (see for instance Liszt & Turner 1978; Ziurys et al. 1991; Ziurys, Hollis & Snyder 1994a; Ziurys et al. 1994b; Halfen, Apponi & Ziurys 2001; Quintana-Lacaci et al. 2013; Codella et al. 2018) – suggesting that these molecules could be present on dust grains, where they would be exposed to radiation processing.

Astronomical observations have shown that CO, O_2, N_2, CH_4, and H_2O molecules can be found on the surface of outer Solar system objects (e.g. Roush 2001; Bieler et al. 2015), where they are irradiated by solar wind and cosmic rays (e.g. Strazzulla &

★ E-mail: dfulvio@puc-rio.br, dfu@oact.inaf.it

Johnson 1991; Palumbo et al. 2008). Thus, even if not yet detected, N—O species can be present on them (e.g. Boduch et al. 2012).

Laboratory experiments have shown (Boduch et al. 2012; Sicilia et al. 2012) that the ion irradiation of a number of different icy mixtures with one component being N_2 ice and the other O_2, CO or H_2O always leads to the appearance of N—O species, such as NO, N_2O, and NO_2. Furthermore, non-energetic surface reaction studies at low temperature showed that NO_2 may form when NO reacts with O, O_2, O_3, or N while NO + H produces hydrogenated species such as HNO and NH_2OH. Similarly, the reaction of NO_2 with H, O, or N may form nitrogen oxides (NO, N_2O, . . .) as well as hydrogenated species (see for instance Congiu et al. 2012; Ioppolo et al. 2014; Minissale et al. 2014)

Despite the number of experimental works in recent years has increased, the chemistry of N—O species is far from being understood. For instance, studies on the effects induced by ion irradiation on solid N_2O, NO_2, and N_2O_4 in space are still scarce. In de Barros et al. (2017), the ion processing of N_2O ices at 11 and 75 K by 90 MeV Xe^{23+} has been reported. Various daughter molecules [NO_2, $(NO)_2$, . . .] were detected and their cross-sections (formation and destruction) were estimated. Similar results were also found and discussed in the recent work by Almeida et al. (2017). Besides these works, there is a lack of dedicated experiments that needs to be filled in. Accordingly, here we present the results of irradiation experiments performed by using 200 keV protons on (i) N_2O ices at 16 and 50 K and (ii) NO_2:N_2O_4 ice mixtures at 16 and 60 K. The experiments were performed at the indicated temperatures to apply the results to a range of case studies, from the ices covering interstellar dust grains to the frozen surface of outer Solar system objects.

2 EXPERIMENTAL APPARATUS

The experiments were executed at the Laboratory for Experimental Astrophysics in Catania (Italy). A vacuum chamber was operated at a pressure $P < 10^{-7}$ mbar and was interfaced to an FTIR spectrometer (Bruker Vertex 70). The spectrometer worked in the range 8000−500 cm^{-1}, 1 cm^{-1} resolution, and 0.25 cm^{-1} sampling. Inside the vacuum chamber, species of interest were inserted (with a gas inlet) and condensed on to a KBr substrate which temperature can be set as low as 16 K. The substrate formed an angle of 45° with the IR beam. In this study, icy samples were condensed at 16 and 50 K (N_2O) and at 16 and 60 K (NO_2:N_2O_4 mixtures). The thickness of the ice accreted on to the substrate was monitored and estimated by using the interference pattern of a laser system (Fulvio et al. 2009). In each experiment, spectra acquired after sample growth (or after irradiation, see below) were divided by the related background spectrum, acquired after the substrate had reached the chosen temperature. In the following, spectra are shown on an optical depth (τ) scale.

For the N_2O frozen films at 16 and 50 K, we used N_2O gas provided by the SIO company. For the frozen mixtures of NO_2:N_2O_4 at 16 and 60 K, we used NO_2 gas (purity $\geq$ 99.5 per cent) provided by the Aldrich company. Taking into account the equilibrium between the NO_2 monomer and its own N_2O_4 dimer, we determined their relative concentration as described in Fulvio et al. (2009). As a first-order approximation, we obtained a mixture of about NO_2:N_2O_4 = 1:1. More details will be given in Section 3.2.

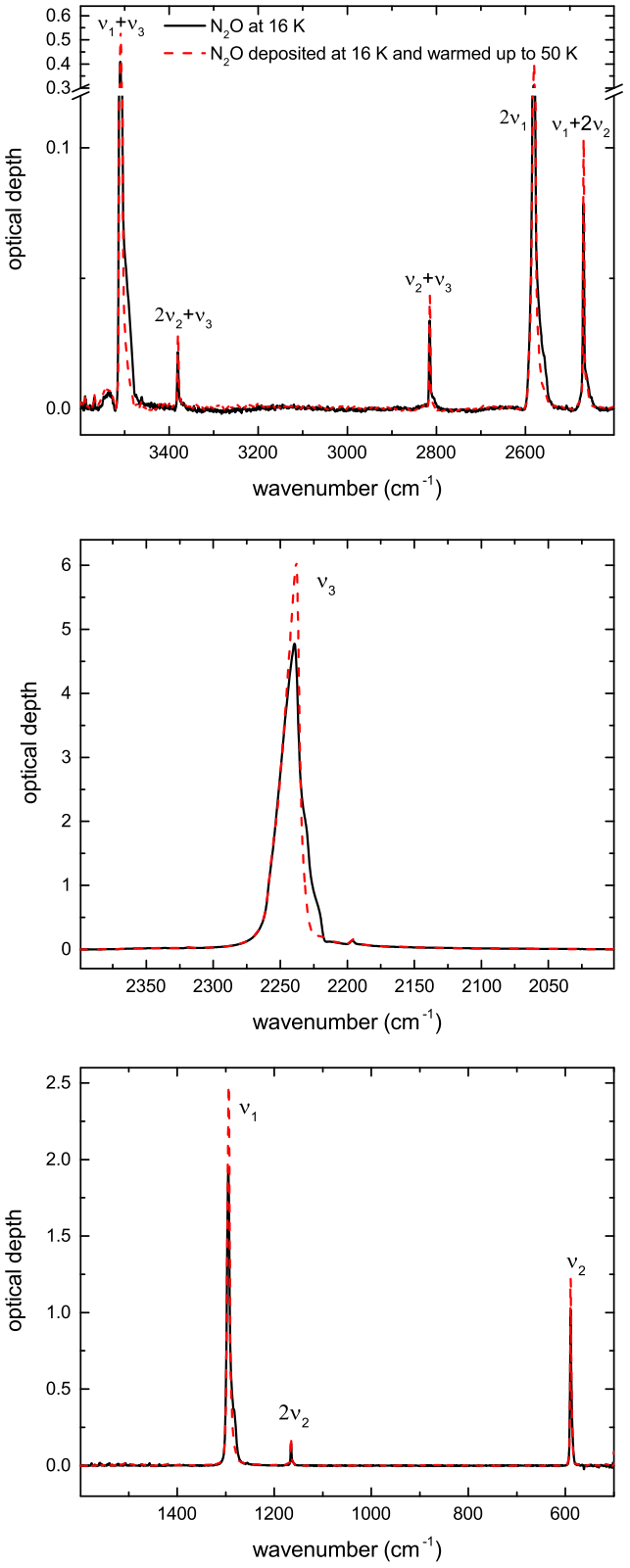

Figure 1. IR spectra of N_2O ices (i) grown at 16 K and (ii) grown at 16 K and warmed up to 50 K.

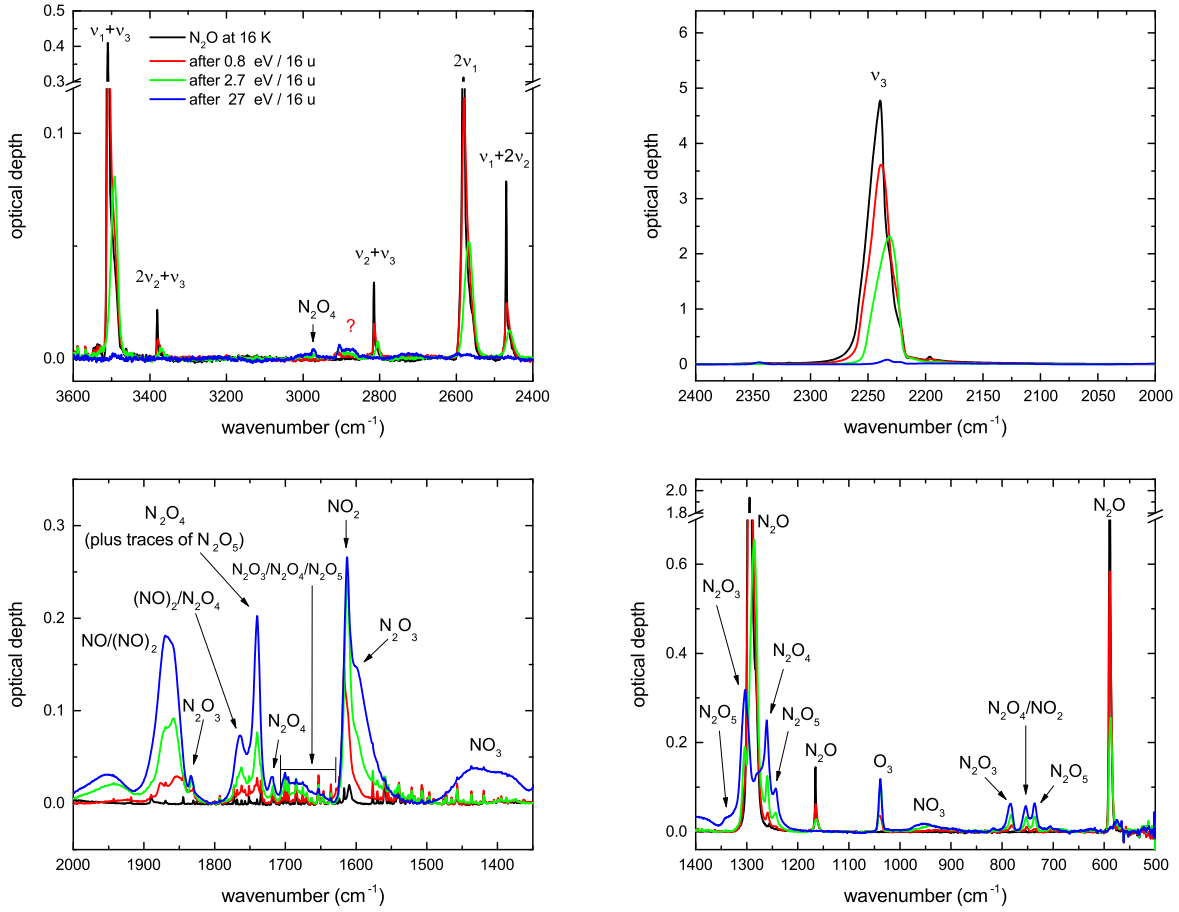

Figure 2. IR spectra of N_2O ice grown at 16 K and after three irradiations (see label at top-left corner). For the sake of clarity four different spectral regions are shown, with optimized *y*-scale. Unidentified bands are indicated with a question mark.

The samples discussed in the current work have been irradiated with 200 keV protons obtained by an ion implanter (Danfysik). By using the SRIM software (Ziegler, Biersack & Ziegler 2008), we estimated stopping powers for both N_2O and NO_2 ices equals to 2.16×10^{-14} eV cm^2 per 16u molecule. Irradiation doses have been determined for each experiment, on a scale of eV per 16u molecule, by multiplying the ion fluence (ions cm^{-2}) and the stopping power (eV cm^2/16u molecule). By using the SRIM software we also checked that for all experiments the ice thickness (usually of about 1 μm) was lower than the ion penetration depth, to guarantee that the sample is irradiated throughout its total thickness. We have checked that the contribution of secondary electrons emitted by the substrate (KBr), in our experimental conditions, is negligible.

More details in Baratta & Palumbo (1998), Baratta, Palumbo & Strazzulla (2000), Palumbo et al. (2006), Fulvio et al. (2009, 2010), Urso et al. (2016), and Baratta & Palumbo (2017).

3 RESULTS

3.1 N_2O ices

IR spectra of N_2O ices (i) as deposited on a KBr substrate at 16 K and (ii) as deposited at 16 K and warmed up to 50 K are presented in Fig. 1. During warm up, we observe a decrease of the width accompanied by an increase of the intensity of the N_2O bands that is due to the amorphous to crystalline transition occurring at 20−30 K (Hudson, Loeffler & Gerakines 2017). Similar modifications of the band's profile have been observed for other solid phase species (such as CO_2, CH_3CN, $HCOOCH_3$) at the relevant temperature (e.g. Modica & Palumbo 2010; Abdulgalil et al. 2013; Baratta & Palumbo 2017). All the main N_2O bands are identified in Table 1.

In Fig. 2, the IR spectra of N_2O ice grown at 16 K after three irradiations (200 keV protons) are shown, in four spectral regions. Similarly, Fig. 3 shows the spectra after three irradiation steps for N_2O ice grown at 16 K and warmed up to 50 K before irradiation. We point out that the actual number of ion irradiation steps performed for this work is way higher than the number of spectra shown in Figs 2 and 3. In fact, these figures want to show just an example of the ion irradiation effects on N_2O ices therefore, for the sake of clarity, we show there only a limited number of spectra. The new molecules appearing after ion irradiation are NO/$(NO)_2$, NO_2, NO_3, N_2O_3, N_2O_4, N_2O_5, O_3. Table 2 lists all new N—O species appearing after ion irradiation, as well as their band positions, assignments, and the band strengths (*A*-value; cm molecules^{-1}) used to calculate the column density *N* (molecules cm^{-2}) of each product (as described, for instance, in Garozzo et al. 2010; equation 1).

The column density evolution for N_2O ices versus the irradiation dose is presented in Fig. 4. To estimate the integrated optical depth values, the band at 2581 cm^{-1} has been used. For N_2O ice irradiated at 16 K, the *A*-value $= 1.5 \times 10^{-18}$ cm mol^{-1} has been used (Fulvio

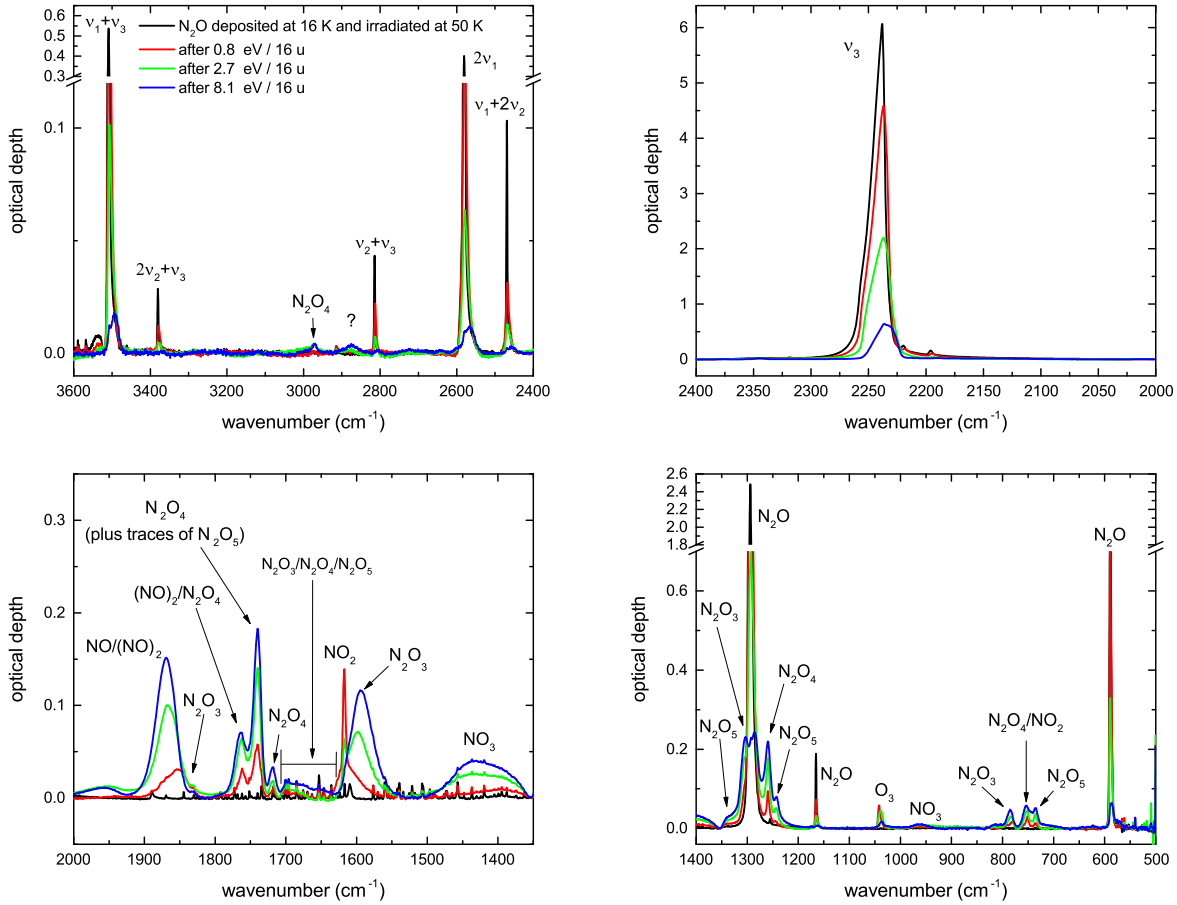

Figure 3. IR spectra of N_2O ice grown at 16 K and irradiated at 50 K. Three ion irradiation steps are also shown (see label in the top-left corner). For the sake of clarity four different spectral regions are shown, with optimized *y*-scale. Unidentified bands are indicated with a question mark.

Table 1. IR bands and assignments of N_2O ice (Fulvio et al. 2009; Hudson et al. 2017).

Wavenumber (cm^{-1})	Mode
589	ν_2
1165	$2\nu_2$
1293	ν_1
2238	ν_3
2469	$\nu_1 + 2\nu_2$
2581	$2\nu_1$
2814	$\nu_2 + \nu_3$
3380	$2\nu_2 + \nu_3$
3509	$\nu_1 + \nu_3$

et al. 2009) while for N_2O ice deposited at 16 K and irradiated at 50 K, the *A*-value = 1.4×10^{-18} cm mol^{-1} (Hudson et al. 2017). Column density evolution is also shown for the following daughter species produced by the ion irradiation: NO, N_2O_3, N_2O_4, and N_2O_5. For the other daughter species appearing in Figs 2 and 3, there are no well-resolved bands to be used or the *A*-values are unknown.

3.2 NO_2:N_2O_4 ice mixtures

IR spectra of the icy mixture NO_2:N_2O_4 = 1:1 grown on a KBr substrate at 16 and 60 K are shown in Fig. 5, in three different spectral regions. Taking into account (i) the equilibrium between the NO_2 monomer and its own N_2O_4 dimer and (ii) the fact that N_2O_4 si-

Table 2. N—O species produced under ion irradiation of N_2O ice at 16 and 50 K, main IR peak positions, assignments, and band strength (*A*-value) used (in bold) to calculate the column density of the produced molecules.

Species	Wavenumber (cm^{-1})	Mode	*A*-value ($\times 10^{-17}$ cm mol^{-1})
NO	**1869**[a,b]	ν_1	**0.68**[f]
$(NO)_2$	1764[a,b]	ν_5	–
	1869[a,b]	ν_1	–
NO_2	753[a,c]	ν_2	–
	1613[a,c]	ν_3	–
NO_3	950[d]	ν_1	–
	1430[d]	–	–
N_2O_3	**785**[a,d]	ν_4	**6.0**[g]
	1305[a,d]	ν_3	–
	1598[a,d]	ν_2	–
	1833[a,d]	ν_1	–
N_2O_4	753[a,d]	ν_{12}	–
	1260[a,d]	ν_{11}	–
	1719[a,d]	ν_7/ν_5	–
	1740[a,d]	ν_9	**0.5**[h]
	1764[a,e]	$\nu_6 + \nu_{11}$	–
N_2O_5	736[a,d]	ν_{11}	–
	1243[a,d]	ν_{10}	**7.4**[f]
	1340[a,d]	ν_2	–

Note. [a]Fateley et al. (1959), [b]Legay & Legay-Sommaire (1995), [c]Shimanouci (1977), [d]Jacox (1998), [e]Andrews & Anderson (1981), [f]Jamieson et al. (2005), [g]de Barros et al. (2017), [h]Fulvio et al. (2009).

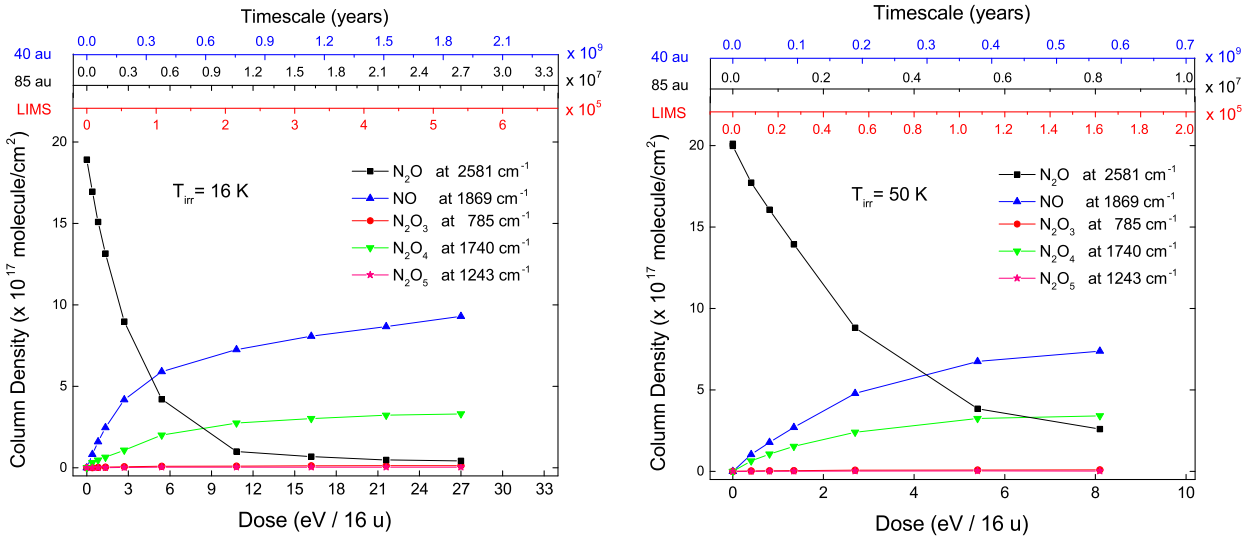

Figure 4. Column density evolution of N_2O ice and daughter molecules (NO, N_2O_3, N_2O_4, and N_2O_5) versus irradiation dose (lower axis) and astrophysical time-scale (upper axis) needed at 40 au, 85 au, and in the local interstellar medium (LISM) to reach those doses, for icy targets 1 μm thick. Irradiations performed at 16 K (left-hand) and at 50 K (right-hand) are shown. Band area values have been estimated by using the IR features indicated in each figure. The *A*-value used for each species is listed in Table 2. Points are connected for clarity.

multaneously shows stable and metastable molecular configurations (which IR features depends on deposition rate and substrate temperature; Fateley, Bent & Crawford 1959), the NO_2 monomer band profile depends on these factors as well. Moreover, additional bands are seen in the deposited ice mixtures, attributed to NO/$(NO)_2$, NO_3, N_2O, N_2 (only at 16 K, as expected with the low desorption temperature of this species, around 30 K), N_2O_3, and CO_2. These are contaminant species inside the lecture bottle, and not in our vacuum system. Indeed they were not present when considering other samples, like for instance N_2O (see Fig. 1). Alternatively, some of them could be formed during the association−dissociation reaction $2NO_2 \leftrightarrow N_2O_4$. In Fig. 5, bands that have not been identified are labelled with a question mark. The identification of the main IR bands of Fig. 5 is reported in Table 3.

In Fig. 6, we show the spectra of the NO_2:N_2O_4 ice mixture deposited at 16 K after three ion irradiations, in three spectral regions. Similarly, Fig. 7 shows the spectra after three irradiation steps for the NO_2:N_2O_4 ice mixture deposited and irradiated at 60 K. As in the case of N_2O ices, we point out that the actual number of ion irradiation steps considered in the following of this work is way higher than the number of spectra shown in Figs 6 and 7. Again, these figures should be seen just as examples of the ion irradiation effects on NO_2:N_2O_4 at 16 and 60 K, respectively, therefore for the sake of clarity, we show only a limited number of spectra. The molecules produced by ion irradiation are NO/$(NO)_2$, N_2O, N_2O_3, N_2O_5, and O_3, while for other molecules already present in the ice before the irradiation we mainly observed a strong change in the band shape and/or peak position (such as for NO_3). In Figs 6 and 7, bands that have not been identified are labelled with a question mark. Table 4 lists all identified N—O species produced by ion irradiation, their band positions, assignments, and band strengths (*A*-value; cm molecule^{-1}) used to calculate the column density of each product.

In Fig. 8, we report the column density versus irradiation dose for the N—O species formed under ion irradiation of the NO_2:N_2O_4 ice mixtures at 16 K (left-hand) and at 60 K (right-hand). The following daughter molecules are shown: NO, N_2O, N_2O_3, and N_2O_5. As discussed in Section 3.1 for the irradiation of N_2O ices, for the other daughter species appearing in Figs 6 and 7 there are unresolved bands or bands for which the *A*-value is unknown. We point out that, unfortunately, this is also true for the two parent molecules present in the starting mixture: NO_2 and N_2O_4. Indeed, despite Fulvio et al. (2009) having estimated the *A*-values for these two molecules at 16 K: (a) for N_2O_4 at 60 K, we already explained there that it is not possible to measure the band area for the feature at 1740 cm^{-1} since the significant and not quantifiable contribution from the contiguous bands should be considered, especially the one at 1765 cm^{-1}; (b) for NO_2, the *A*-values reported in Fulvio et al. (2009) are overestimated since the authors did not consider the contribution due to N_2O_3 to the area of the band at 1613 cm^{-1}. The data analysis performed for the current study gave us the opportunity to understand this.

Therefore, we could not estimate the column density evolution versus irradiation dose for either NO_2 or N_2O_4. Nevertheless, in Fig. 9 (right-hand) we show the normalized band area evolution for N_2O_4 versus irradiation dose. This is the N_2O_4 decreasing as irradiation proceeds, at two irradiation temperatures, 16 and 60 K. Similarly, in Fig. 9 (left-hand) we report the normalized band area evolution for N_2O, at the two irradiation temperatures considered in this study (Section 3.1): 16 and 50 K. Experimental data shown in Fig. 9 were fitted by using the following equation:

$$y = y_\infty + (1 - y_\infty)\, e^{-\sigma\, Dose}, \quad (1)$$

where y_∞ is the asymptotic normalized band area, σ is the cross-section in 16u eV^{-1}, and *Dose* is in eV/16u. Best-fitting parameters are reported in Table 5. Often in the literature cross-sections are given in units of cm^2. If we indicate with σ the cross-sections in 16u eV^{-1} units given in Table 5 and with SP the stopping power in eV cm^2/16u molecule, the cross-sections σ_{cm^2} in standard units of cm^2 can be obtained for 200 keV protons through the relation: $\sigma_{cm^2} = \sigma \times SP = \sigma \times 2.16 \times 10^{-14}$. We have verified with several experiments that fast ions of different mass and energy give similar

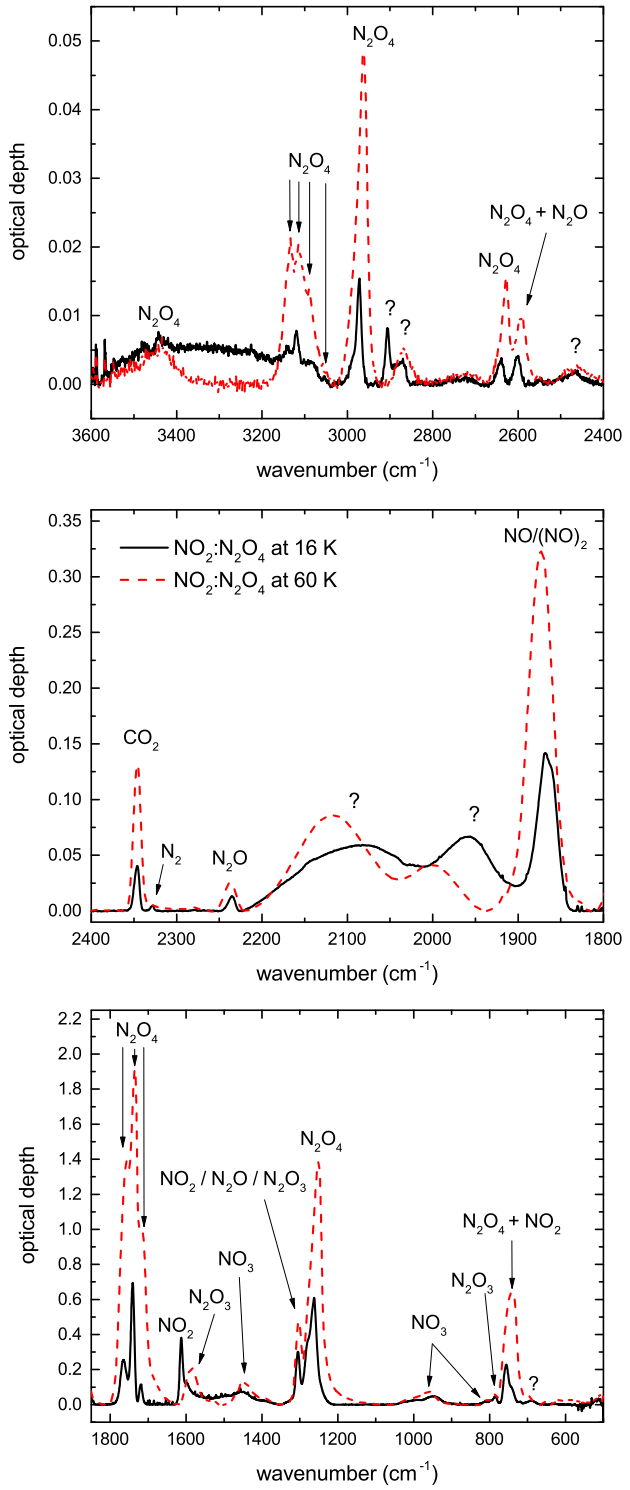

Figure 5. IR spectra of the icy mixture NO_2:N_2O_4 = 1:1 at 16 and 60 K. Unidentified bands are indicated with a question mark.

chemical effects in ices, provided that the exposure dose is the same. Hence, unlike the cross-sections given in cm^2 units, which depend on the stopping power, the cross-sections given in 16u eV^{-1} units are, in first approximation, independent of the particular ion considered. Thus, a comparison with other experimental studies and the extrapolation to astrophysical environments is straightforward.

From Fig. 9 and Table 5, we can see that the destruction of N_2O_4 by ion irradiation (right-hand) is almost independent of the temperature, with small differences only at the beginning of the irradiation where N_2O_4 at 16 K is destroyed faster than at 60 K. Once irradiation reaches higher doses it looks like the maximum amount of N_2O_4 destroyed by ion irradiation is equal to about 70 per cent, independently of temperature. This means that equilibrium is reached among the N_2O_4 destruction and re-formation rates, where its re-formation is due to the ion processing of the daughter species that meanwhile have increased their concentration within the irradiated ice. Even more interesting is the case of ion irradiation of N_2O (left-side of Fig. 9). We point out that when irradiating the N_2O ice at 50 K we had to stop the irradiation experiment at a lower dose than in the experiment at 16 K. As a consequence, at 50 K we only have data for the beginning of the irradiation and we did not consider fitting the data in this case. Nevertheless, it looks like, where available, the two set of data are superimposed (within the uncertainties of the measurements) and the fitting of the experimental data at 16 K works quite well also for the data at 50 K. In other words, the destruction of N_2O by ion irradiation seems independent of the ice temperature in the range investigated. Another interesting aspect is that the amount of N_2O destroyed by ion irradiation at the maximum dose reached in our experiments is about 98 per cent, i.e. the N_2O ice is almost entirely destroyed.

4 ASTROPHYSICAL IMPLICATIONS AND CONCLUSIONS

It is well known that fast ions (keV−MeV) colliding with frozen samples release their energy along the ion track causing the formation of molecular fragments and radicals which recombine quickly (one picosecond or less) giving rise to molecular species not present in the original sample. As a consequence original species are destroyed and the chemical composition of the samples may be significantly modified.

The destruction of frozen N_2O, NO_2, and N_2O_4 induced by ion irradiation in space is still scarcely understood and with the current work we want to contribute to fill in this void. For this, we have presented the results of ion irradiation experiments of (i) N_2O ices at 16 and 50 K and (ii) NO_2:N_2O_4 ice mixtures at 16 and 60 K. The experiments were performed at the indicated temperatures to comprehend a large range of case studies, from the ices covering interstellar grains to the frozen surface of the outer Solar system objects.

The results presented in the current study show that irradiation of N_2O at 16 or 50 K produces similar effects. The most abundant molecules appearing after ion irradiation are $NO/(NO)_2$, NO_2, NO_3, N_2O_3, N_2O_4, N_2O_5, O_3 (Figs 2 and 3). Among the daughter species, NO and N_2O_4 are the main products, independently of the irradiation temperature, while N_2O_3 and N_2O_5 are seen only in small amounts (Fig. 4). Similarly, ion irradiation of NO_2:N_2O_4 ice mixture at 16 or 60 K produces comparable effects as well. The most abundant molecules produced by ion irradiation are $NO/(NO)_2$, N_2O, N_2O_3, N_2O_5, and O_3 (Figs 6 and 7). Among the daughter species, NO is again the main product, independently of the irradiation temperature, while N_2O_3, N_2O, and N_2O_5 are detected only in small amounts (Fig. 8). In addition, the experiments suggest that in neither N_2O_4 nor N_2O does the temperature of the ice play a crucial role when analysing the destruction rate of the parent species. The amount of N_2O_4 and N_2O destroyed by ion irradiation within the maximum dose reached in our experiments is equal to about 70 and 98 per cent, respectively (Fig. 9). For a detailed discussion on the reaction network which drives the destruction of N—O species and the formation of daughter molecules the reader is referred to

Table 3. Feature assignment for the N—O species seen on the spectra of the NO_2:N_2O_4 ice mixture deposited at 16 or 60 K, before ion irradiation (Fig. 5). Only identified bands are here reported.

Wavenumber (cm^{-1}) at 16 – at 60 K	Mode	Species	References
755 – 742	ν_{12}; ν_2	N_2O_4; NO_2	(a), (d); (a), (c)
785	ν_4	N_2O_3	(a), (d)
805	–	NO_3	(d)
947 – 960	ν_1	NO_3	(d)
1263 – 1251	ν_{11}	N_2O_4	(a), (d)
1307 – 1303	ν_1; ν_1; ν_3	NO_2; N_2O; N_2O_3	(a); (g); (a), (d)
1453 – 1443	–	NO_3	(d)
1585	ν_2	N_2O_3	(a), (d)
1613	ν_3	NO_2	(a), (c)
1720 – 1716	ν_7/ν_5	N_2O_4	(a), (d)
1741 – 1734	ν_9	N_2O_4	(a), (d), (e)
1765 – 1755	$\nu_6 + \nu_{11}$; ν_5	N_2O_4; $(NO)_2$	(a), (e); (a), (b)
1868 – 1873	ν_1; ν_1	NO; $(NO)_2$	(a), (b); (a), (b)
2235 – 2237	ν_3	N_2O	(g)
2601 – 2592	$\nu_1 + \nu_{11}$; $2\nu_1$	N_2O_4; N_2O	(h); (g)
2640 – 2627	$2\nu_7 + \nu_{11}$	N_2O_4	(h)
2970 – 2960	$\nu_5 + \nu_{11}$	N_2O_4	(h)
3055	$\nu_1 + \nu_9$	N_2O_4	(h)
3084 – 3090	$\nu_1 + \nu_9 + R$	N_2O_4	(h)
3120 – 3114	$2\nu_7 + \nu_9$	N_2O_4	(h)
3140 – 3134	$2\nu_7 + \nu_9 + R$	N_2O_4	(h)
3442	$\nu_5 + \nu_9/\nu_5 + \nu_9 + R$	N_2O_4	(h)

Note. [a]Fateley et al. (1959), [b]Legay & Legay-Sommaire (1995), [c]Shimanouci (1977), [d]Jacox (1998), [e]Andrews & Anderson (1981), [f]Jamieson et al. (2005), [g]Fulvio et al. (2009), [h]Wiener & Nixon (1957), R = torsional lattice vibrations.

dedicated works such as Almeida et al. (2017) and de Barros et al. (2017).

To understand the astrophysical implications of the experiments here presented, we compared the dose range covered in the performed experiments with the irradiation dose suffered by surfaces in the outer Solar system and the ISM and, eventually, with the astrophysical time-scale of surface processing in these regions. By considering that the main contribution to the flux of energetic particles in the mentioned regions is due to solar energetic particles and galactic cosmic ray ions and by using the data reported in Strazzulla et al. (2003) and Cooper et al. (2003), we have estimated the astrophysical time-scale needed in the outer Solar system, at 40 and 85 au, and in the local interstellar medium (LISM) to accumulate those doses for icy targets 1 μm thick. We point out that the choice of these three locations has been to cover a broad range of possible case studies, in the outer Solar system and beyond. The results of these calculations are shown in Figs 4 and 8 for the experiments on N_2O and NO_2:N_2O_4, respectively. Similarly, Fig. 9 shows the normalized band area evolution for N_2O and N_2O_4 as a function of doses and astrophysical time-scale.

From Figs 4 and 8 we can see that ion irradiation of N_2O ices and NO_2:N_2O_4 ice mixtures can form quite large amounts of NO in time-scales of 10^5–10^8 yr. In addition, from Fig. 9 we can also see that the destruction of N_2O and N_2O_4 (and reasonably of its monomer NO_2) by ion irradiation is quite a fast process, occurring on time-scales of about 10^5–10^8 yr as well. Taking into account the irradiation experiments performed on H_2O:N_2, H_2O:N_2:O_2, N_2:O_2, and CO:N_2 where NO always appears among the main produced species (Boduch et al. 2012; Sicilia et al. 2012), the results of the current study on the formation of NO and destruction of the other N—O species suggest that NO ice is the main candidate which should be looked for in IR astronomical spectra of interstellar grain mantles, comets, and outer Solar system objects.

Combining the results presented here with those reported in Sicilia et al. (2012), it is possible to conclude that the solid NO feature at about 1870 cm^{-1} (5.35 μm) is potentially detectable in young stellar objects (YSOs). In fact the expected abundance of NO produced after ion processing of icy grain mantles is of the order of 10^{-2} with respect to carbon monoxide (e.g. Sicilia et al. 2012). Assuming that the fractional abundance of CO is 10^{-4} (Frerking, Langer & Wilson 1982; Wilson & Rood 1994), then the fractional abundance of solid NO would be 10^{-6}. Being the column density of hydrogen towards YSOs of the order of 10^{22}–10^{23} molecules cm^{-2} (Tielens et al. 1991), then it is expected a column density for solid NO of the order of 10^{16}–10^{17} molecules cm^{-2}. Using the A-value reported in Table 2 this corresponds to a band area, in optical depth scale, ranging from 0.068 to 0.68 cm^{-1}. The full width at half-maximum (FWHM) of the NO band will depend on the mixture the molecule is embedded in. For CO-rich or N_2-rich mixtures, the FWHM of the NO band is about 2 cm^{-1}. As a consequence the optical depth at peak position would range from 0.3 to 0.03. These values are above the detection limit of the MIRI instrument aboard the *James Webb Space Telescope* (*JWST*; Wells et al. 2015). Furthermore, the NO feature at about 1870 cm^{-1} is not expected to be superposed to other bands due to more abundant species.

As concerns the other N—O species studied in this work, the most intense NO_2 band which falls around 1615 cm^{-1} is superposed to the strong H_2O band at 1660 cm^{-1} and would be very hardly detectable. The main N_2O band occurs around 2240 cm^{-1}. It is superposed to the broad HNCO band at about 2260 cm^{-1} which is also expected to be present in the spectra taken towards YSOs (e.g. Fedoseev et al. 2018). A quantitative estimation of the expected column density of N_2O in icy grain mantles is not straightforward. In fact it has been shown that N_2O is also formed in variable amount after energetic processing of other ice mixtures, like for instance CO:CH_4:N_2,

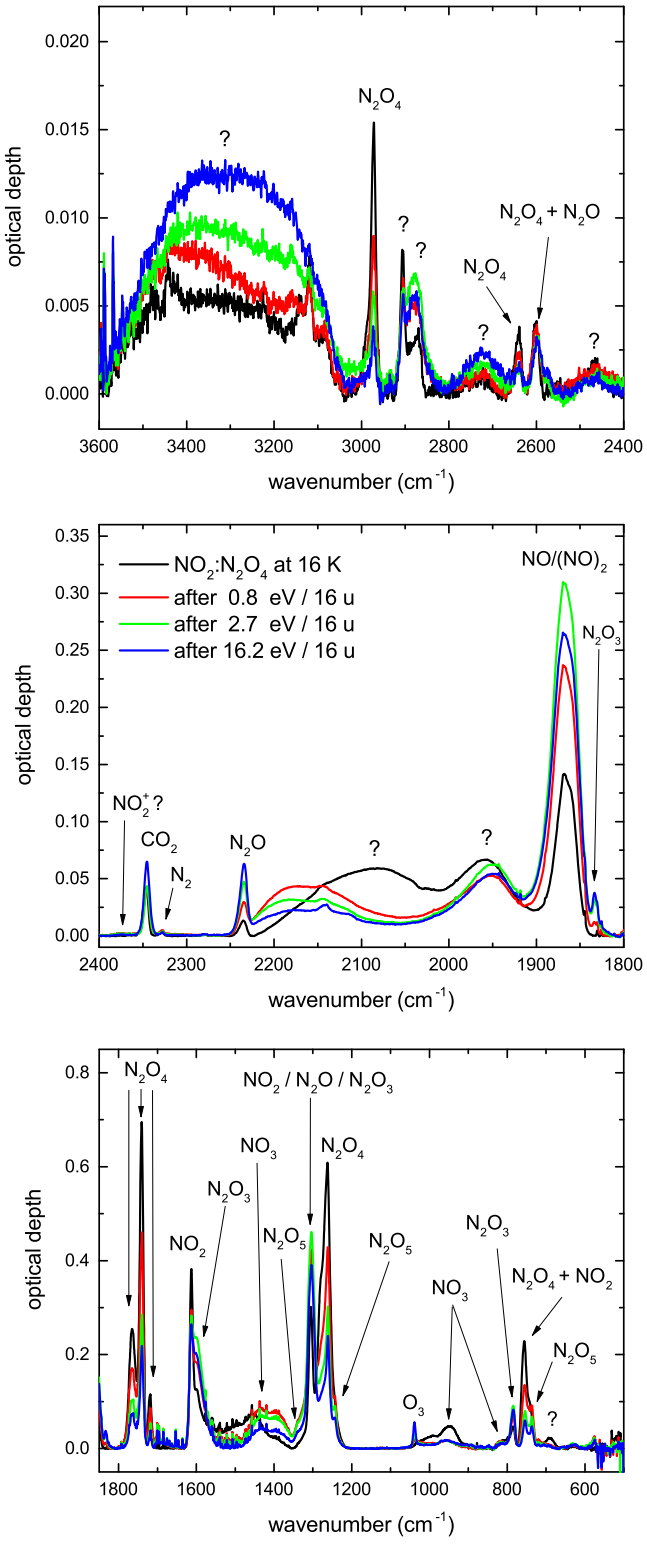

Figure 6. IR spectra of the icy mixture NO_2:N_2O_4 deposited at 16 K and after three irradiations (see label). For the sake of clarity three different spectral regions are shown, with optimized *y*-scale. Unidentified bands are indicated with a question mark.

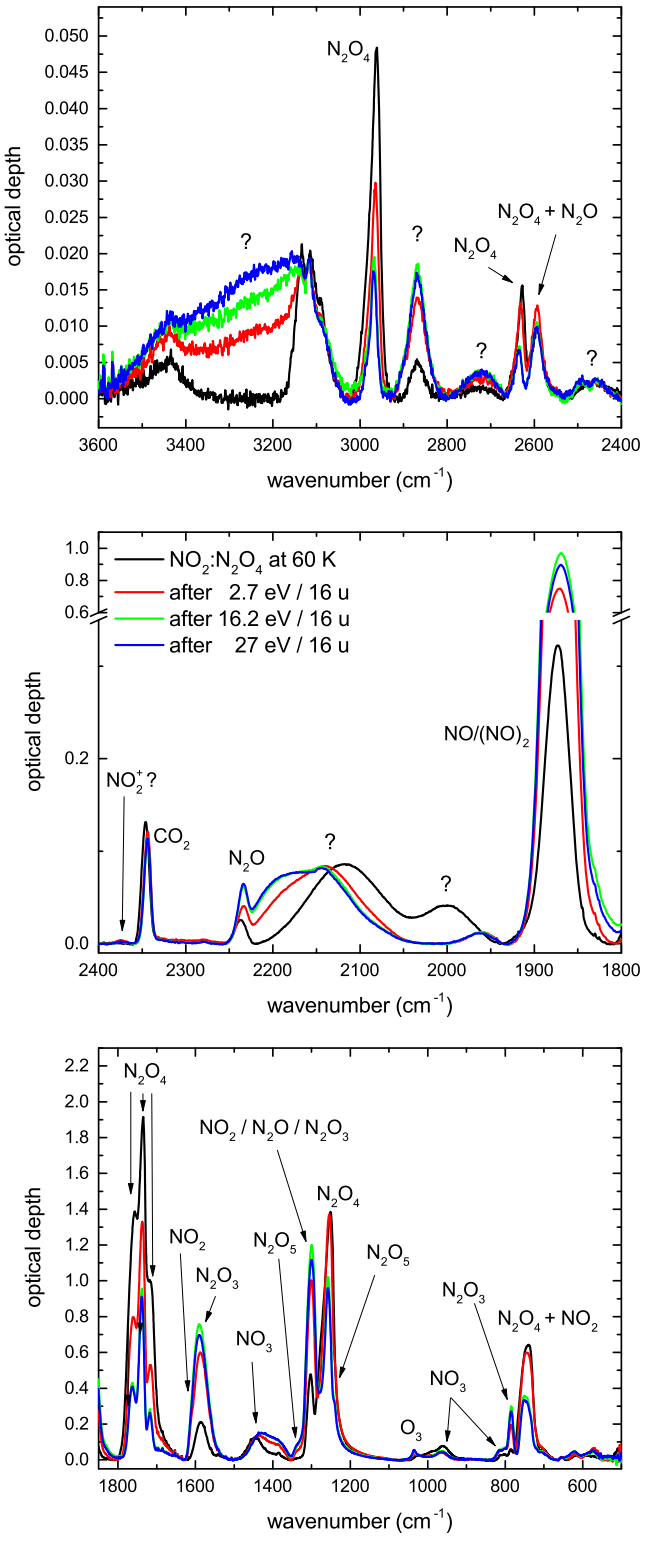

Figure 7. IR spectra of the icy mixture NO_2:N_2O_4 deposited at 60 K and after three ion irradiations (see label). For the sake of clarity three different spectral regions are shown, with optimized *y*-scale. Unidentified bands are indicated with a question mark.

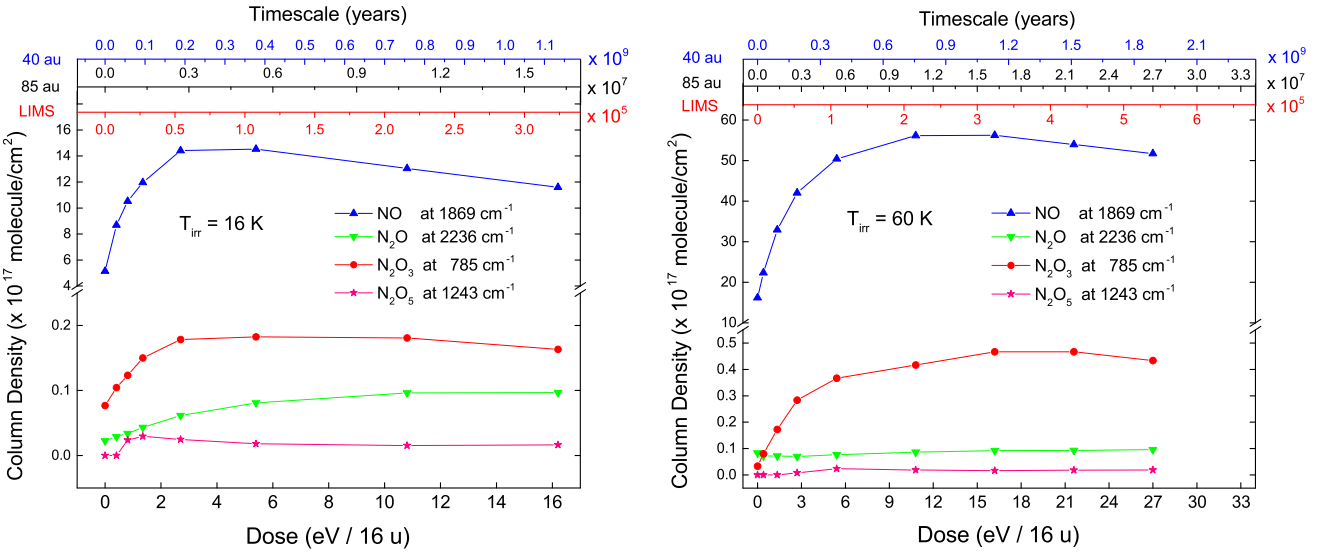

Figure 8. Column density evolution for the N—O species formed under ion irradiation of the icy mixture NO_2:N_2O_4 versus irradiation dose (lower axis) and astrophysical time-scale (upper axis) needed at 40 au, 85 au, and in the LISM to reach those doses, for icy targets 1 μm thick. Irradiations performed at 16 K (left-hand) and at 60 K (right-hand) are shown. Band area values have been estimated by using the IR features indicated in each figure. The *A*-value used for each species is listed in Table 4. Points are connected for clarity.

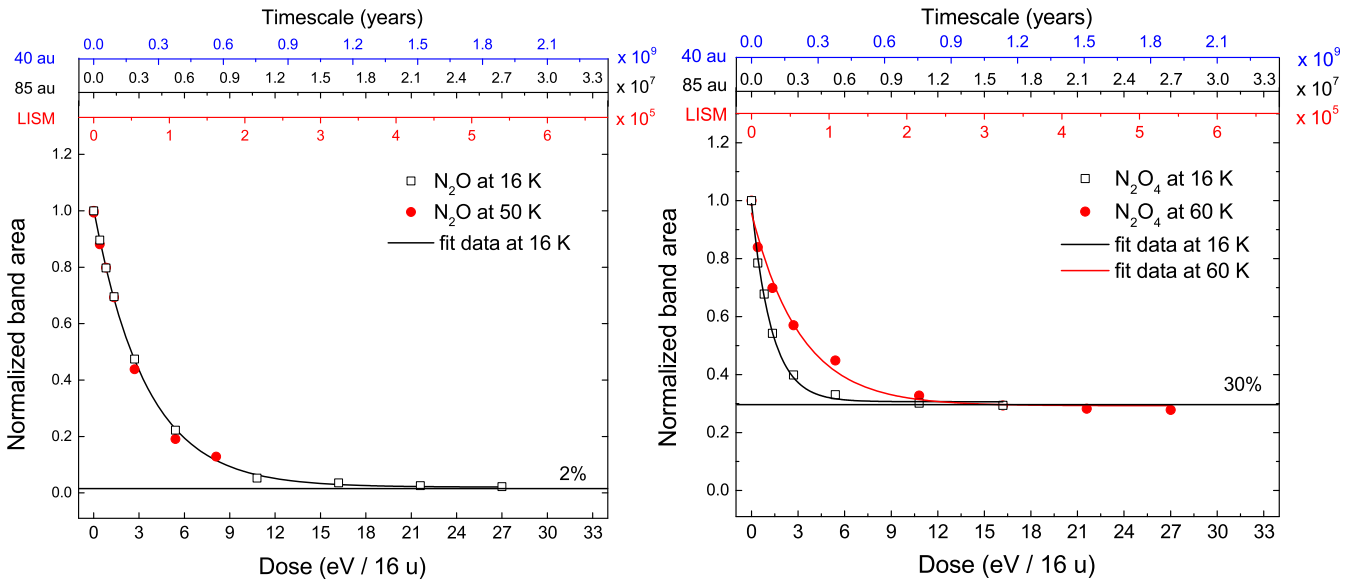

Figure 9. Normalized band area decreasing for N_2O ices (left-hand) and N_2O_4 ices (right-hand) versus irradiation dose (lower axis) and astrophysical time-scale (upper axis) needed at 40 au, 85 au, and in the LISM to reach those doses, for icy targets 1 μm thick. Two irradiation temperatures were considered for each species. Data were fitted by equation (1): $y = y_\infty + (1 - y_\infty)\,e^{-\sigma\,Dose}$. Fits are shown with solid curves.

H_2O:CH_4:N_2, CH_3OH:N_2 (e.g. Baratta et al. 2015; Fedoseev et al. 2018). If detected by the *JWST*, the intensity of the N_2O band with respect to the NO and HNCO features could give insights about the starting composition of icy grain mantles.

To the best of our knowledge, the bands due to N—O species cannot be detected with current IR telescopes. In fact, the wavelength value of 5.35 μm is outside the range (1–5 μm) of the VLT-ISAAC and Gemini-NIRI spectrographs. The *Spitzer Space Telescope* IRS spectrograph covered the spectral region at about 5.35 μm with low resolution ($R = \lambda/\Delta\lambda \sim 100$) and low signal-to-noise ratio S/N = 50−100 (e.g. Houck et al. 2004; Boogert et al. 2008; Öberg et al. 2011). These values are significantly lower than the values which will be reached with the *JWST* ($R = 1500-3000$ and S/N = 100−300). As a consequence, presently, no conclusions can be drawn on the presence of NO in icy grain mantles. Moreover, the N_2O band at 2240 cm^{-1} (4.46 μm) is not accessible by ground-based telescopes because of telluric absorption and it is outside the range observable with *Spitzer*.

Table 4. N—O species formed under ion irradiation of the NO_2:N_2O_4 ice mixture at 16 and 60 K, main IR peak positions, assignments, and band strength (*A*-value) used (in bold) to calculate the column density of the produced molecules.

Species	Wavenumber (cm^{-1})	Mode	*A*-value ($\times 10^{-17}$ cm mol^{-1})
NO	**1869**[a,b]	ν_1	**0.68**[e]
$(NO)_2$	1764[a,b]	ν_5	–
	1869[a,b]	ν_1	–
N_2O	1305[c]	ν_1	–
	2236[c]	ν_3	at 16 K = **5.7**[c]; at 60 K = **5.1**[f]
	2599[c]	$2\nu_1$	–
N_2O_3	**785**[a,d]	ν_4	**6.0**[g]
	1305[a,d]	ν_3	–
	1598[a,d]	ν_2	–
	1833[a,d]	ν_1	–
N_2O_5	736[a,d]	ν_{11}	–
	1243[a,d]	ν_{10}	**7.4**[e]
	1340[a,d]	ν_2	–

Note. [a]Fateley et al. (1959), [b]Legay & Legay-Sommaire (1995), [c]Fulvio et al. (2009), [d]Jacox (1998), [e]Jamieson et al. (2005), [f]Hudson et al. (2017), [g]de Barros et al. (2017).

Table 5. Best-fitting parameters of the experimental data shown in Fig. 9, by using equation (1).

	N_2O – 16 K	N_2O_4 – 16 K	N_2O_4 – 60 K
y_∞	0.020 ± 0.004	0.306 ± 0.008	0.292 ± 0.017
σ (16u eV^{-1})	0.288 ± 0.005	0.778 ± 0.04	0.318 ± 0.037

To date, only NO, HNO, and N_2O have been identified in the ISM and then only in gas phase (see for instance Quintana-Lacaci et al. 2013; Codella et al. 2018). Despite NO_2 has been extensively searched, it has not been detected so far (Halfen et al. 2001). NO is expected to be formed in the gas phase at an abundance comparable to the observed values while chemical models and recent low-temperature laboratory experiments showed that icy NO could be efficiently 'consumed' by addition of H atoms to produce hydrogenated species (Charnley et al. 2001; Congiu et al. 2012) or by addition of $O/O_2/O_3$ or N atoms to produce NO_2 (Minissale et al. 2014). Thus, detecting N—O species on to ISM grain mantles and measuring their abundances will help us to better understand the chemical evolution of molecules with the N—O bond in space.

ACKNOWLEDGEMENTS

Authors thank F. Spinella for his help with the experiments. DF acknowledges the Brazilian foundation CNPq ('Bolsa de Produtividade em Pesquisa, PQ 2015' – Processo: 309964/2015−6 and 'Chamada Universal 2016' – Processo: 426929/2016−0) and FAPERJ ('Programa Jovem Cientista do Nosso Estado 2017' – Processo: E−26/203.204/2017) for financial support. BS would like to acknowledge the British Council RXP Award and INSPIRE Grant (IFA−11CH−11). AB is grateful to the Brazilian agencies CNPq (301868/2017−4) and CAPES (BEX 5383/15−3). This work was partly supported by the Italian Ministero dell'Istruzione, dell'Università e della Ricerca through the grant Progetti Premiali 2012 – iALMA (CUP C52I13000140001). Part of this work is part of the Europlanet 2020 RI which has received funding from the European Union's Horizon 2020 research and innovation programme under grant agreement no. 654208.

REFERENCES

Abdulgalil A. G. M. et al., 2013, Phil. Trans. R. Soc. A, 371, 20110586
Almeida G. C., Pilling S., de Barros A. L. F., da Costa C. A. P., Pereira R. C., da Silveira E. F., 2017, MNRAS, 471, 1330
Andrews B., Anderson A., 1981, J. Chem. Phys., 74, 1534
Baratta G. A., Palumbo M. E., 1998, J. Opt. Soc. Am. A, 15, 3076
Baratta G. A., Palumbo M. E., 2017, A&A, 608, A81
Baratta G. A., Palumbo M. E., Strazzulla G., 2000, A&A, 357, 1045
Baratta G. A., Chaput D., Cottin H., Fernandez Cascales L., Palumbo M. E., Strazzulla G., 2015, Planet. Space Sci., 118, 211
Bieler A. et al., 2015, Nature, 526, 678
Boduch P., Domaracka A., Fulvio D., Langlinay T., Lv X. Y., Palumbo M. E., Rothard H., Strazzulla G., 2012, A&A, 544, A30
Boogert A. C. A. et al., 2008, ApJ, 678, 985
Boogert A. C. A., Gerakines P. A., Whittet D. C. B., 2015, ARA&A, 53, 541
Charnley S. B., Rodgers S. D., Ehrenfreund P., 2001, A&A, 378, 1024
Codella C. et al., 2018, MNRAS, 474, 5694
Congiu E. et al., 2012, ApJ, 750, L12
Cooper J. F., Christian E. R., Richardos J. D., Wang C., 2003, Earth, Moon Planets, 92, 261
Cottin H. et al., 2008, Adv. Space Res., 42, 2019
de Barros A. L. F., da Silveira E. F., Fulvio D., Boduch P., Rothard H., 2017, MNRAS, 465, 3281
Fateley W. G., Bent H. A., Crawford B., Jr, 1959, J. Chem. Phys., 31, 204
Fedoseev G., Scirè C., Baratta G. A., Palumbo M. E., 2018, MNRAS, 475, 1819
Frerking M. A., Langer W. D., Wilson R. W., 1982, ApJ, 262, 590
Fulvio D., Sivaraman B., Baratta G. A., Palumbo M. E., Mason N. J., 2009, Spectrochim. Acta A, 72, 1007
Fulvio D., Guglielmino S., Favone T., Palumbo M. E., 2010, A&A, 511, A62
Fulvio D., Raut U., Baragiola R. A., 2012, ApJ, 752, L33
Fulvio D., Góbi S., Jäger C., Kereszturi Á., Henning Th., 2017, ApJS, 233, 14
Garozzo M., Fulvio D., Kanuchova Z., Palumbo M. E., Strazzulla G., 2010, A&A, 509, A67
Garrod R. T., Weaver S. L. W., 2013, Chem. Rev., 113, 8939
Gerakines P. A., Schutte W. A., Ehrenfreund P., 1996, A&A, 312, 289
Halfen D. T., Apponi A. J., Ziurys L. M., 2001, ApJ, 561, 244
Houck J. R. et al., 2004, ApJS, 154, 18
Hudson R. L., Loeffler M. J., Gerakines P. A., 2017, J. Chem. Phys., 146, 024304.
Ioppolo S., Fedoseev G., Minissale M., Congiu E., Dulieu F., Linnartz H., 2014, Phys. Chem. Chem. Phys., 16, 8270
Jacox M. E., 1998, J. Phys. Chem. Ref, Data, 27, 115
Jamieson C. S., Bennett C., Mebel A. M., Kaiser R. I., 2005, ApJ, 624, 436
Kaiser R. I., Roessler K., 1998, ApJ, 503, 959
Legay F., Legay-Sommaire N., 1995, J. Chem. Phys., 102, 7798
Liszt H. S., Turner B. E., 1978, ApJ, 224, L73
Minissale M., Fedoseev G., Congiu E., Ioppolo S., Dulieu F., Linnartz H., 2014, Phys. Chem. Chem. Phys., 16, 8257
Modica P., Palumbo M. E., 2010, A&A, 519, A22
Öberg K. I. et al., 2011, ApJ, 740, 109
Palumbo M. E., Strazzulla G., 1993, A&A, 269, 568
Palumbo M. E., Baratta G. A., Collings M. P., McCoustra M. R. S., 2006, Phys. Chem. Chem. Phys., 8, 279
Palumbo M. E., Baratta G. A., Fulvio D., Garozzo M., Gomis O., Leto G., Spinella F., Strazzulla G., 2008, J. Phys.: Conf. Ser., 101, 012002
Qi C. et al., 2013, Science, 341, 630
Quintana-Lacaci G., Agúndez M., Cernicharo J., Bujarrabal V., Sánchez Contreras C., Castro-Carrizo A., Alcolea J., 2013, A&A, 560, L2
Raut U., Famá M., Loeffler M. J., Baragiola R. A., 2008, ApJ, 687, 1070
Raut U., Fulvio D., Loeffler M. J., Baragiola R. A., 2012, ApJ, 752, 159
Roush T. L., 2001, J. Geophys. Res., 106, 33315
Shimanouci T., 1977, J. Phys. Chem. Ref. Data, 6, 993

Sicilia D., Ioppolo S., Vindigni T., Baratta G. A., Palumbo M. E., 2012, A&A, 543, A155.
Strazzulla G., Johnson R. E., 1991, in, Newburn R. L., Neuegebauer M., Rahe J., eds, Comets in the post-Halley Era, Vol. 1, Springer, Dordrecht. p. 243
Strazzulla G., Cooper J. F., Christian E. R., Johnson R. E., 2003, C. R. Phys., 4, 791
Tielens A. G. G. M., Tokunaga A. T., Geballe T. R., Baas F., 1991, ApJ, 381, 181
Urso R. G., Scirè C., Baratta G. A., Compagnini G., Palumbo M. E., 2016, A&A, 594, A80
Wells M. et al., 2015, PASP, 127, 646
Wiener R. N., Nixon E. R., 1957, J. Chem. Phys., 26, 906
Wilson T. L., Rood R., 1994, ARA&A, 32, 191
Ziegler J. F., Biersack J. P., Ziegler M. D., 2008, The Stopping and Range of Ions in Solids. Pergamon, New York, p. 321
Ziurys L. M., McGonagle D., Minh Y., Irvine W. M., 1991, ApJ, 373, 535
Ziurys L. M., Hollis J. M., Snyder L. E., 1994a, ApJ, 430, 706
Ziurys L. M., Apponi A. J., Hollis J. M., Snyder L. E., 1994b, ApJ, 436, L181

This paper has been typeset from a TEX/LATEX file prepared by the author.